OPEN

Citation: Bone Research (2014) 2, 14006; doi:10.1038/boneres.2014.6

www.boneresearch.org

ARTICLE

LRP6 in mesenchymal stem cells is required for bone formation during bone growth and bone remodeling

Changjun Li[1], Bart O Williams[2], Xu Cao[1] and Mei Wan[1]

Lipoprotein receptor-related protein 6 (LRP6) plays a critical role in skeletal development and homeostasis in adults. However, the role of LRP6 in mesenchymal stem cells (MSCs), skeletal stem cells that give rise to osteoblastic lineage, is unknown. In this study, we generated mice lacking LRP6 expression specifically in nestin$^+$ MSCs by crossing *nestin-Cre* mice with *LRP6^{flox}* mice and investigated the functional changes of bone marrow MSCs and skeletal alterations. Mice with LRP6 deletion in nestin$^+$ cells demonstrated reductions in body weight and body length at 1 and 3 months of age. Bone architecture measured by microCT (μCT) showed a significant reduction in bone mass in both trabecular and cortical bone of homozygous and heterozygous LRP6 mutant mice. A dramatic reduction in the numbers of osteoblasts but much less significant reduction in the numbers of osteoclasts was observed in the mutant mice. Osterix$^+$ osteoprogenitors and osteocalcin$^+$ osteoblasts significantly reduced at the secondary spongiosa area, but only moderately decreased at the primary spongiosa area in mutant mice. Bone marrow MSCs from the mutant mice showed decreased colony forming, cell viability and cell proliferation. Thus, LRP6 in bone marrow MSCs is essential for their survival and proliferation, and therefore, is a key positive regulator for bone formation during skeletal growth and remodeling.

Bone Research (2014) **2,** 14006; doi:10.1038/boneres.2014.6; Published online 29 April 2014

INTRODUCTION

Low-density lipoprotein receptor-related protein 6 (LRP6), a member of the low-density lipoprotein receptor-related family, was initially identified as a coreceptor of Wnts and promote canonical Wnt signaling.[1–5] Recent human and animal genetic studies indicate that LRP6 is a key regulator for skeletal development and bone homeostasis in adults.[6–13] Wnt triggers a number of different intracellular signaling cascades and the particular pathways triggered by a Wnt binding to its receptor complex is determined by the two co-receptors, LRP5 and 6, involved in the initial engagement. LRP5 and 6 are transmembrane proteins whose large extracellular domains are highly related. The role of LRP5 was emphasized by the discovery of some patients with either high or low bone mass phenotypes, caused by activating and loss-of-function mutations of LRP5, respectively.[14–17] The role of LRP6 in regulating skeletal homeostasis is less studied. It was reported that a single missense mutation in *LRP6*R611C that underlies autosomal dominant early onset coronary artery disease and osteoporosis in a very large outlier Iranian kindred.[6] Recently, the same group identified three novel mutations in 200 white Americans with early onset familial coronary artery disease and osteoporosis, indicating the involvement of LRP6 in regulating bone metabolism.[7] From mouse genetic studies, LRP6 seems to have both distinct and overlapping functions with LRP5 in bone. *Lrp6*$^{-/-}$ mice are embryonic lethal and display defects in both limb and axial development.[2,10] As with *Lrp5*, haploinsufficiency for *Lrp6* results in reduced bone mass, but also worsens *Lrp5* deficiency-induced osteopenia in double-mutant mice, demonstrating that the functions of these two receptors are not fully redundant.[10–11,18–19] Importantly, two recent studies in the mice with osteoblast-specific LRP6 deletion demonstrated that LRP6 in mature osteoblasts is required for osteoblastic differentiation and the maintenance of bone homeostasis.[12–13]

Bone homeostasis depends on the concerted activities of bone cells. Bone cells such as osteoblasts and osteoclasts must proliferate, migrate, attach, spread and

[1]Department of Orthopaedic Surgery, Johns Hopkins University School of Medicine, Baltimore, MD 21205, USA and [2]Center for Skeletal Disease and Tumor Metastasis and Laboratory of Cell Signaling and Carcinogenesis, Van Andel Research Institute, Grand Rapids, MI, USA
Correspondence: M Wan (mwan4@jhmi.edu)
Received: 20 December 2013; Revised: 15 January 2014; Accepted: 31 January 2014; Uncorrected proof published 9 April 2014

differentiate from precursor cells originating from mesenchymal or hematopoietic stem cells. Osteoblasts were shown to be non-replicative.[20] An adequate supply of osteoblasts from their precursors, bone marrow mesenchymal stem cells (MSCs), is critical to bone formation. The fact that skeletal development proceeds normally in embryos that lack either *Lrp5* or *Lrp6* in the skeletogenic mesenchyme, which contain precursors for the skeletal tissues,[21] suggests that LRP5 and LRP6 redundantly regulate osteoblastogenesis and skeletal development, and individual LRP5 or 6 is not essential for embryonic bone development. Whether MSC-specific LRP6 is important in the maintenance of bone mass in postnatal bone growth and bone remodeling in adults is not characterized.

MSCs are clonogenic populations that present in heterogeneity within the bone marrow. The challenge is that no defined *in vivo* markers are able to label the entire MSC population. Nestin is an intermediate filament protein that was originally identified as a marker of neural progenitors.[22] It has recently been reported that, transgenes that use control regions from the nestin gene mark early cells in the osteoblast lineage with a perivascular location.[23] Sorting for nestin-GFP cells, the cells carrying green fluorescent protein under the control of nestin gene regulatory regions, in adult bone yielded all the bone's colony-forming unit - fibroblast (CFU-F), some of which expressed markers of osteoblastic, adipogenic and chondrogenic differentiation. The number of these nestin-GFP cells increased after 5 weeks of parathyroid hormone (PTH) administration. Further, when a nestin-cre$^{ER T}$ transgene was activated by administration of tamoxifen in 3-month-old mice, osteoblasts, osteocytes and chondrocytes were marked after a prolonged chase using a reporter gene. This study suggests that nestin-Cre$^{ER T}$ marks bone marrow MSCs that have both self-renewal and multilineage potential *in vivo*. In the present study, we generated a mouse model, in which LRP6 is selectively ablated in nestin^{+} cells by crossing *nestin-Cre* mice with *Lrp^{flox}* mice. We demonstrated that LRP6 expression in nestin^{+} MSCs affected their survival, proliferation and colony-forming capacity, resulting in skeletal defects in both bone growth and bone remodeling.

MATERIALS AND METHODS

Animals

Lrp6$^{f/f}$ mice were obtained from Van Andel Research Institute.[21,24] Transgenic mice expressing the Cre recombinase under the control of human nestin promoter (*nestin-Cre*) were purchased from Jackson Lab. Homozygous *Lrp6$^{f/f}$* mice were crossed with *nestin-Cre* transgenic mice to generate double heterozygous *nestin-Cre$^{+/-}$; Lrp6$^{wt/f}$* mice, which were then mated with *Lrp6$^{f/f}$* mice to generate control *Cre$^{-/-}$; Lrp6$^{f/f}$* mice (named '*Lrp6$^{+/+}$*' hereafter), heterozygous deletion *Cre$^{+/-}$; Lrp6$^{wt/f}$* mice (named '*Lrp6$^{+/-}$*' hereafter) and homozygous deletion *Cre$^{+/-}$; Lrp6$^{f/f}$* mice (named '*Lrp6$^{-/-}$*' hereafter). All animals were maintained in the Animal Facility of the Johns Hopkins University School of Medicine. The experimental protocol was reviewed and approved by the Institutional Animal Care and Use Committee of the Johns Hopkins University (Baltimore, MD, USA). Genomic DNA was extracted from tail snips with phenol/chloroform. Genotyping of the animals was achieved by PCR for Cre recombinase (5′-GCG GTC TGG CAG TAA AAA CTA TC-3′ and 5′-GTG AAA CAG CAT TGC TGT CAC TT-3′) and the loxP sites (5′-GGG GTT CTA CTT TTG TGT GTG G-3′ and 5′- CCG TCT GTT TGC ATA AAG CAA CA-3′).

Antibodies

Primary antibodies including goat anti-LRP6 (Abcam, Cambridge, MA, USA), anti-nestin (Aves Labs, Tigard, OR, USA), rabbit anti-osterix (Abcam, Cambridge, MA, USA), rabbit anti-osteocalcin (Takara, Otsu, Shiga, Japan) and anti-5-bromo-2′-deoxyuridine (BrdU) (Abcam, Cambridge, MA, USA) were used for immunohistochemical analysis. Secondary antibodies for immunohistochemistry were from Jackson ImmunoResearch (West Grove, PA, USA).

Analysis of skeletal phenotypes

Mice were anesthetized by inhalation of 2.5% isoflurane (Abbott Laboratories, Abbott Park, IL, USA) mixed with O_2 (1.5 L·min^{-1}). For microCT (μCT) analysis, femora obtained from mice were dissected free of soft tissue, fixed overnight in 70% ethanol and analyzed by a high resolution μCT (SkyScan1076 *in-vivo* CT; SKYSCAN Company, Kontich, Belgium). Image Reconstruction software (NRecon v1.6), data analysis software (CTAn v1.9) and three-dimensional model visualization software (CTVol v2.0) were used to analyze parameters of the trabecular bone in the metaphysis and mid-diaphyseal cortical bone. The scanner was set at a voltage of 50 kVp, a current of 201 μA and a resolution of 12.63679 μm per pixel. Cross-sectional images of the distal femur were used to perform three-dimensional histomorphometric analysis of trabecular bone. The sample area selected for scanning was a 3.0-mm length of the metaphyseal trabecular bone immediately subjacent to the growth plate. Cortical morphometry was analyzed within a 600 μm long section at mid-diaphysis of the femur and included measurements of average thickness and cross-sectional area.

For histochemistry, immunohistochemistry and histomorphometric analysis, the femora were resected and fixed in phosphate-buffered saline (pH 7.4) containing 4% paraformaldehyde for 48 h, decalcified in 10% ethylenediamine tetraacetic acid (pH 7.0) for 14 days and embedded in paraffin. Four-μm-thick longitudinally

oriented sections of bone including the metaphysis and diaphysis were processed for hematoxylin–eosin and immunohistochemical staining. For static histomorphometry, measurements of two-dimensional parameters of the trabecular bone were performed with OsteoMeasureXP Software (OsteoMetrics, Inc., Decatur, GA, USA). The sample area selected for calculation was a 1 mm^2 area within the metaphyseal trabecular bone. All sections were observed on Olympus BX51 microscope (Olympus, Tokyo, Japan).

Immunohistochemistry analysis was performed using standard protocol as the manufacturer recommended (EnVision System; Dako, Carpinteria, CA, USA). Briefly, the bone sections were processed for antigen retrieval by digestion in 0.05% trypsin (pH 7.8) for 15 min at 37 ℃, and then incubated with antibodies against LRP6 (diluted 1:50), osteocalcin (Ser463/465) (diluted 1:100) and osterix (diluted 1:400) overnight at 4 ℃. An horseradish peroxidase (HRP)-streptavidin detection system (Dako, Carpinteria, CA, USA) was subsequently used to detect the immunoactivity followed by counterstaining with hematoxylin (Sigma, St. Louis, MO, USA). Sections incubated with 1% non-immune serum phosphate buffered solution (PBS) solution served as negative controls. For immunofluorescence staining, sections were incubated with first antibodies (anti-LRP6, anti-nestin or anti-BrdU) followed by incubation with fluorescein isothiocyanate-conjugated or Cy3-conjugated secondary antibodies (Jackson ImmunoResearch). Nuclei were counterstained with 4′,6-diamidino-2-phenylindole. (Sigma). The sections were mounted with the ProLong Antifade Kit (Molecular Probes, Eugene, OR, USA) and observed under a confocal microscope (FLUOVIEW FV300; Olympus, Tokyo, Japan).

Measurements of serum osteocalcin and crosslinked C-terminal telopeptide of type 1 collagen (CTX-I)

Serum bone formation marker osteocalcin and bone resorption marker CTX-I, were measured using commercial kits: Mouse Osteocalcin EIA Kit (Biomedical technologies, Inc. Stoughton, MA) and Mouse CTX-I ELISA Kit (MyBioSource, Inc., San Diego, CA, USA) according to the manufacturer's instructions.

CFU-F assays of bone marrow MSCs

Bone marrow cells were collected from wild-type (WT), heterozygous and homozygous LRP6-deficient mice euthanized by cervical dislocation. For CFU-F assays, at the time of euthanasia, bone marrow from femoral, tibial and humeral medullary cavities were collected, and cell numbers were determined after removal of red blood cells with Zapoglobin (Coulter Corp., Miami, FL, USA). The numbers of CFU-Fs in murine bone marrow isolates were determined in cocultures with irradiated guinea pig marrow cells, as reported.[25]

Isolation of murine bone marrow MSCs and *in vitro* deletion of LRP6

At the time of euthanasia, bone marrow from femoral, tibial and humeral medullary cavities of WT mice were collected, and cell numbers were determined after removal of red blood cells with Zapoglobin (Coulter Corp.). Cells aliquots were incubated for 20 min at 4 ℃ with phycoerythrin-, fluorescein isothiocyanate-, peridinin chlorophyll protein- and allophycocyanin-conjugated antibodies against mouse Sca-1, CD29, CD45 and CD11b (Bio-Legend, San Diego, CA, USA). Acquisition was performed on a fluorescence-activated cell sorting Aria model (BD Biosciences, San Jose, CA, USA), and analysis was performed with a fluorescence-activated cell sorting DIVE software version 6.1.3 (BD Biosciences). The sorted $CD29^+Sca\text{-}1^+CD45^-CD11b^-$ MSCs were enriched by further culture. To eliminate LRP6 from the cells, cultured MSCs were infected with control adenovirus (Ad-GFP) or Cre recombinase virus M1 (Ad-CreM1) (Vector Laboratories, Burlingame, CA, USA) at a multiplicity of infection of 100 for most experiments.

Population doubling time, cell viability and proliferation assays

After infected with adenovirus, MSCs were cultured for two passages (P2) before analysis. Population doubling times were calculated between P1 and P2 as t/n, where t is the duration of culture in days and n is the number of population doublings calculated by using the formula $n=(\log N_h-\log N_i)/\log 2$, where N_h is the number of cells harvested at the time of counting at P2 and N_i is the number of cells initially plated at P1). To test the viability of the cells, 1×10^5 of MSCs infected with adenovirus were seeded into six-well plates. The cells were trypsinised after 48 h of culture using 1 mL of 0.25% trypsin. A 1:2 dilution of the cells in Trypan Blue (T8154; Sigma-Aldrich, St. Louis, MO, USA) was made and transferred onto a coverslipped haemocytometer. Using phase-contrast light microscopy, viable cells were identified as rounded and bright, whereas blue cells were considered nonviable. A cell count and the calculation of percentage viability were recorded. To test the proliferation capacity of the cells, 1×10^5 of MSCs infected with adenovirus were seeded into each chambered slide and incubated for 24 h, 5 mL of 10 mmol·L^{-1} BrdU was added into the media and incubated for 2 h. Cells were then fixed with methonal. Immunohistochemistry analysis was performed using mouse anti-BrdU as described above.

Statistical analysis

All data were presented as mean±s.e.m. For comparison of histomorphometric parameters in WT and KO mice, Student's *t*-test was used. For quantitative analysis of immunostaining data, Student's *t*-test was performed followed by Chi-square test. Significant level was defined as $P<0.05$.

RESULTS

Mice with LRP6 deletion in nestin$^+$ MSCs acquire a low bone mass phenotype

Double heterozygous *nestin-Cre*$^{+/-}$; *Lrp6*$^{wt/flox}$ mice were crossed with *Lrp6*$^{flox/flox}$ mice (Figure 1a) to generate four genotypes of mice: *Cre*$^{-/-}$; *Lrp6*$^{flox/flox}$ (*Lrp6*$^{+/+}$), *Cre*$^{-/-}$; *Lrp6*$^{wt/flox}$, heterozygous deletion *Cre*$^{+/-}$; *Lrp6*$^{wt/flox}$ (*Lrp6*$^{+/-}$) and homozygous deletion *Cre*$^{+/-}$; *Lrp6*$^{flox/flox}$ (*Lrp6*$^{-/-}$). All four different genotypes of mice were born at the expected Mendelian frequency, and the survival of

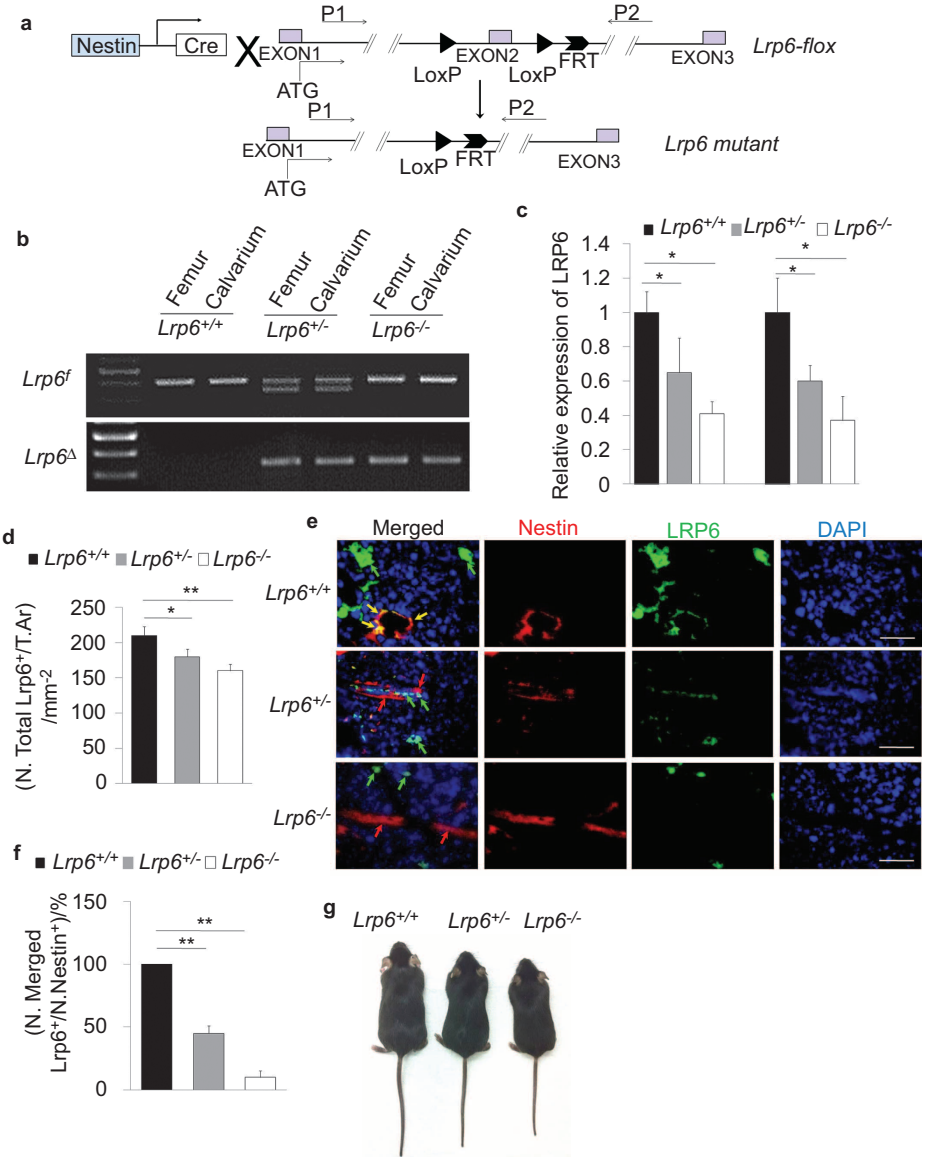

Figure 1. Generation and characterization of *Nestin-Cre; LRP6*$^{f/f}$ *mice*. (**a**) Schematic diagram to generate *Nestin-Cre* transgenic mice on *Lrp6-flox* background. LoxP sites in *Lrp6* gene are indicated by dark triangles. Primers used for the allele-specific PCR in panel **b** are indicated by black arrows. (**b** and **c**) Expression of LRP6 in bone tissues from male *Cre*$^{-/-}$; *LRP6*$^{F/f}$ (*Lrp6*$^{+/+}$), *Cre*$^{+/-}$; *Lrp6*$^{wt/f}$ (*Lrp6*$^{+/-}$) and *Cre*$^{+/-}$; *Lrp6*$^{f/f}$ (*LRP6*$^{-/-}$) mice tested by genomic PCR (**b**) and qRT-PCR (**c**). The bands in upper panel represent the insertion of *loxP* site in exons 2. The bands in lower panel show Cre-mediated recombination of the *Lrp6*^{flox} allele only occurred in bone tissue of *Lrp6*$^{+/-}$ and *Lrp6*$^{-/-}$ mice. The primers used for the PCR amplification in upper and lower panels were indicated in **a**. (**d–f**) Immunohistochemical analysis of LRP6 expression in femur sections of 3-month-old male *Lrp6*$^{+/+}$ *Lrp6*$^{+/-}$ and *Lrp6*$^{-/-}$ mice. Number of total LRP6-positive cells per mm^2 tissue area (N.LRP6$^+$ cells/T.Ar) (**d**). Representative double-immunofluorescence staining of LRP6 (green) and nestin (red) in femur sections from 3-month-old male *Lrp6*$^{+/+}$, *Lrp6*$^{+/-}$ and *Lrp6*$^{-/-}$ mice (**e**). Nuclei were counterstained with DAPI (blue). Yellow arrows, perivascular nestin$^+$ cells that express LRP6; green arrows, nestin$^-$ cells that express LRP6; red arrows, nestin$^+$ cells that do not express LRP6. Scale bars=100 μm. Quantitative analysis of the percentage of nestin$^+$LRP6$^+$ double=positive cells out of total nestin$^+$ cells (**f**). A total of three femur sections from each mouse and five mice per treatment group were analyzed. *P<0.05, **P<0.001, *vs.* *Lrp6*$^{+/+}$ group. (**g**) Representative images showing the sizes of 3-month-old male mice with different genotypes. DAPI, 4′,6-diamidino-2-phenylindole; qRT-PCR, quantitative reverse transcriptase-PCR.

all *Lrp6*-deficient mice was indistinguishable from that of control mice ($Cre^{-/-}$; $Lrp6^{flox/flox}$ and $Cre^{-/-}$; $Lrp6^{wt/flox}$). Analysis of genomic DNA confirmed that deletion of exons 2, which encode the *Lrp6* domain, occurred efficiently in bone tissue such as femur and calvarium (Figure 1b). Heterozygous $Lrp6^{+/-}$ and homozygous $Lrp6^{-/-}$ mice exhibited approximately 40% and 60% reduction, respectively, in LRP6 expression levels in mRNA in bone tissue as detected by quantitative reverse transcriptase-PCR analysis (Figure 1c). We also assessed whether nestin$^+$ MSCs-derived bone cells lost LRP6 expression by immunohistochemical analysis of femur tissue sections using an antibody against LRP6. The reduction in total LRP6$^+$ cells were observed in bone tissue of $Lrp6^{+/-}$ and $Lrp6^{-/-}$ mice compared with those in WT littermates (Figure 1d). Notably, almost all the perivascular nestin$^+$ cells (in red) expressed LRP6 (in green) in femur tissue of WT mice (Figure 1e, overlapped red cells and green cells, and Figure 1f). Perivascular nestin$^+$ cells in bone marrow of $Lrp6^{+/-}$ and $Lrp6^{-/-}$ mice, however, lost LRP6 expression (Figure 1e, red cells only), even though other types of cells in bone marrow still express LRP6 in these mice (Figure 1e, green cells only). The results suggest that LRP6 is successfully knocked out in nestin$^+$ MSCs. $Lrp6^{+/-}$ and $Lrp6^{-/-}$ mice of both sexes initially appeared normal, but they were smaller than WT littermates at 1 month and 3 months after birth as quantified by body weight, body length, and tail length (Figure 1g and Table 1). Mice expressing Cre only did not exhibit any skeletal abnormality relative to WT mice in deferent studies[26–27] and no abnormal phenotype was observed in our analysis.

To examine the bone phenotypes in the mutant mice, we performed a longitudinal analysis of bone architecture using μCT. Both male $Lrp6^{+/-}$ and $Lrp6^{-/-}$ mice showed reduced trabecular bone volume, thickness and number, and increased trabecular space at 3 months of age compared to WT littermates, and the reduction was more pronounced in $Lrp6^{-/-}$ mice (Figure 2). Notably, BV/TV reduced >50% (Figure 2b) and the trabecular number reduced >40% (Figure 2d) in $Lrp^{-/-}$ mice relative to WT mice. Female $Lrp6^{+/-}$ mice and $Lrp6^{-/-}$ mice exhibit similar changes in all these parameters compared to female WT littermates (Figure 2f–2j). Cortical bone architecture in the mutant mice of both sexes was also altered significantly (Figure 3). Cortical tissue area was reduced more than 20% in male (Figure 3b) and 15% in female mutant mice (Figure 3f) relative to controls. Cortical bone thickness was reduced by approximately 10% in both sexes (Figure 3d and 3h). The results suggest that LRP6 deficiency in nestin$^+$ cells results in low bone mass in both trabecular and cortical bone during postnatal bone growth and bone remodeling in adults.

Mice with LRP6 deletion in nestin$^+$ MSCs show decreased osteoblastic bone formation

As the phenotypic changes of the skeleton in mutant mice are quite similar in male and female, we then analyzed the changes of osteoblasts and osteoclasts in bone of male mice. We chose 3-month-old mice, which is considered as the late growth phase when the longitudinal bone growth still remains and bone remodeling is already active.[28] The primary spongiosa area and secondary spongiosa area of a long bone represent active areas of bone growth/modeling and remodeling, respectively. Bone histomorphometric analyses revealed a more than 70% reduction in osteoblast number per bone perimeter and more than 75% reduction in osteoblast surface per bone surface at the secondary spongiosa area of femur, bone remodeling active area, from mutant mice relative to WT mice (Figure 4e and 4f). The reductions in osteoblast numbers at the primary spongiosa area of femur of the mutant mice were much less pronounced (Figure 4a and 4b). The results indicate that MSC-specific LRP6 positively regulates osteoblastogenesis during bone remodeling. Decreases in osteoclast numbers at the primary and secondary spongiosa area of femur from mutant mice *vs.* WT mice were also observed, but the changes were much less compared with the changes of osteoblast numbers (Figure 4c, 4d, 4g and 4h). We also performed tartrate-resistant acid phophatase (TRAP) staining in the femoral

Table 1. Baseline phenotype in 1-month-old and 3-month-old $Lrp6^{+/+}$, $Lrp6^{+/-}$ and $Lrp6^{-/-}$ mice

	Male			Female		
Parameter	$Lrp6^{+/+}$ (n=10)	$Lrp6^{+/-}$ (n=10)	$Lrp6^{-/-}$ (n=10)	$Lrp6^{+/+}$ (n=10)	$Lrp6^{+/-}$ (n=10)	$Lrp6^{-/-}$ (n=10)
1-month-old mice						
Body mass/g	24.50±3.04	21.85±1.73*	14.17±2.4*	21.65±2.33	15.9±0.61*	13.67±3.8*
Body length/cm	16.15±1.67	15.00±0.71*	12.86±1.46*	17.00±1.41	13.77±0.40*	13.50±1.29*
Tail length/cm	7.25±1.06	6.65±0.50*	5.86±0.85*	8.00±0.71	6.33±0.23*	6.11±0.64*
3-month-old mice						
Body mass/g	30.53±2.60	27.90±1.43*	23.7±1.12*	22.35±1.52	19.35±0.97*	18.30±0.80*
Body length/cm	17.00±0.39	16.00±0.41*	15±0.46*	17.00±0.25	15.00±0.21*	15.00±0.29*
Tail length/cm	7.87±0.16	6.70±0.24*	6.50±0.35*	8.00±0.16	6.85±0.43*	6.75±0.14*

Values presented are mean±s.e.m.
* P<0.05 versus Lrp6$^{+/+}$.

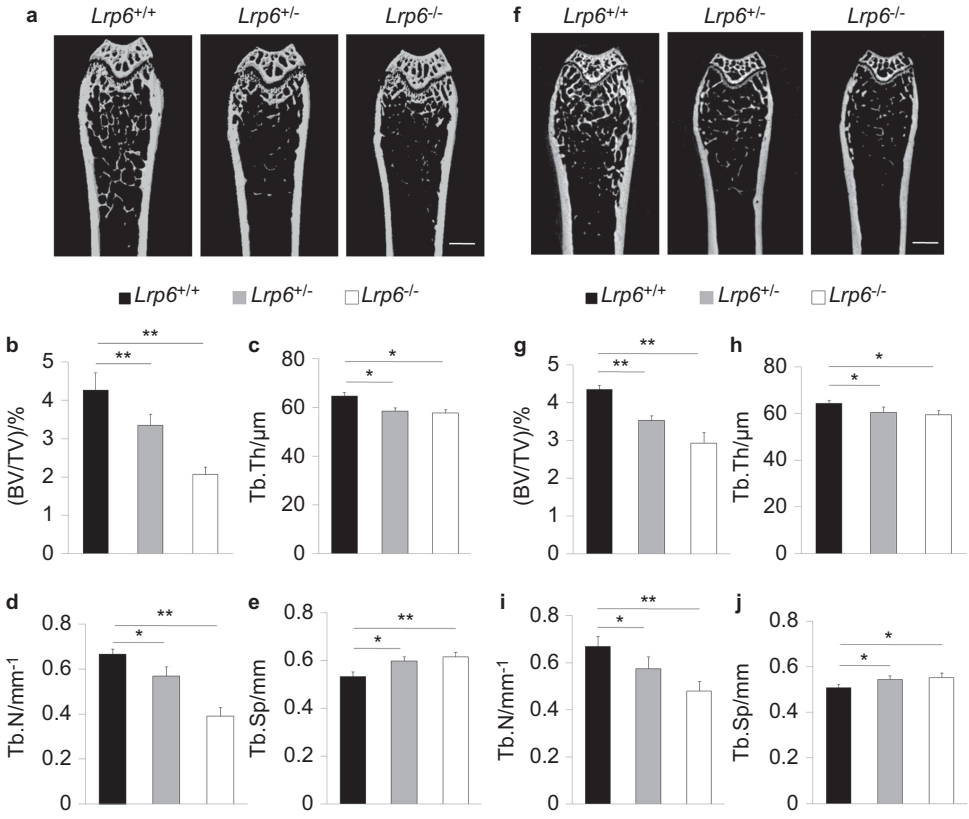

Figure 2. Mice with LRP6 deletion in nestin$^+$ MSCs exhibit low bone mass in trabecular bone. (**a**) Representative μCT images of the trabecular bone area of distal femur from 3-month-old male *Lrp6*$^{+/+}$, *Lrp6*$^{+/-}$ and *Lrp6*$^{-/-}$ mice. Scale bar=500 μm. (**b–e**) Quantitative analysis of the trabecular bone area of distal femur from 3-month-old male *Lrp6*$^{+/+}$, *Lrp6*$^{+/-}$ and *LRP6*$^{-/-}$ mice. Trabecular bone volume fraction (BV/TV%) (**b**), trabecular thickness (Tb.Th) (**c**), trabecular number (Tb.N) (**d**) and trabecular separation (Tb.Sp) (**e**). (**f**) Representative μCT images and quantitative analysis of the trabecular bone area of distal femur from 3-month-old female mice. Scale bar=500 μm. (**g–j**) Quantitative analysis of the trabecular bone area of distal femur from 3-month-old female *Lrp6*$^{+/+}$ *Lrp6*$^{+/-}$ and *LRP6*$^{-/-}$ mice. Trabecular bone volume fraction (BV/TV%) (**g**), trabecular thickness (Tb.Th) (h), trabecular number (Tb.N) (**i**) and trabecular separation (Tb.Sp) (**j**). n=10, *P<0.01, **P<0.001, *vs.* *Lrp6*$^{+/+}$ group.

sections of these mice. Consistent with the results of histomorphometry analysis, the numbers of TRAP-positive osteoclasts on the trabecular bone surface of *Lrp6*$^{+/-}$ and *Lrp6*$^{-/-}$ mice were also reduced compared to WT mice (Figure 4i-4l). We also measured the serum levels of the bone formation marker osteocalcin and the bone resorption marker CTX-I in the mice. Reduced serum concentrations of osteocalcin but unchanged serum concentration of CTX-I were detected in both *Lrp6*$^{+/-}$ and *Lrp6*$^{-/-}$ mice relative to WT mice (Figure 4m and 4n). As the activities of bone-forming osteoblasts and bone-resorptive osteoclasts are well coupled during bone remodeling, our results suggest that LRP6 deficiency in nestin$^+$ MSCs primarily caused dramatic reduction in osteoblastic bone formation, which may in turn affected the osteoclastic bone resorption activitiy.

Bone marrow MSCs are skeletal stem cells that give rise to osteoblastic lineage of cells.[23] We next examined whether LRP6 deletion in osteoblasts affects the number of osterix-positive (Osx$^+$) cells, which are osteoblast-deriving osteoprogenitors, and osteocalcin-positive (Ocn$^+$) mature osteoblasts, by immunohistochemical analysis. A dramatic reduction in the numbers of Osx$^+$ cells in secondary spongiosa area of femora were detected in the mutant mice relative to WT littermates (>80% in Figure 5c and 5d). Similarly, Ocn$^+$ mature osteoblasts on bone surface of the secondary spongiosa area of femora in mutant mice were also dramatically reduced. Ocn$^+$ cell number in homozygous *Lrp6*$^{-/-}$ mice was only 18% of those in WT mice (Figure 5g and 5h). Interestingly, the numbers of both Osx$^+$ cells and Ocn$^+$ cells at the primary spongiosa were not changed significantly relative to those of WT littermates (Figure 5a, 5b, 5e and 5f), indicating a primary role of LRP6 in regulating the function of MSCs during bone remodeling. Taken together, these results, in combination of the fact of smaller bone observed in 1-month-old mice, suggest that LRP6 is required for the functional maintenance of bone marrow MSCs and consequent bone formation in both bone growth in young mice and bone remodeling in adults.

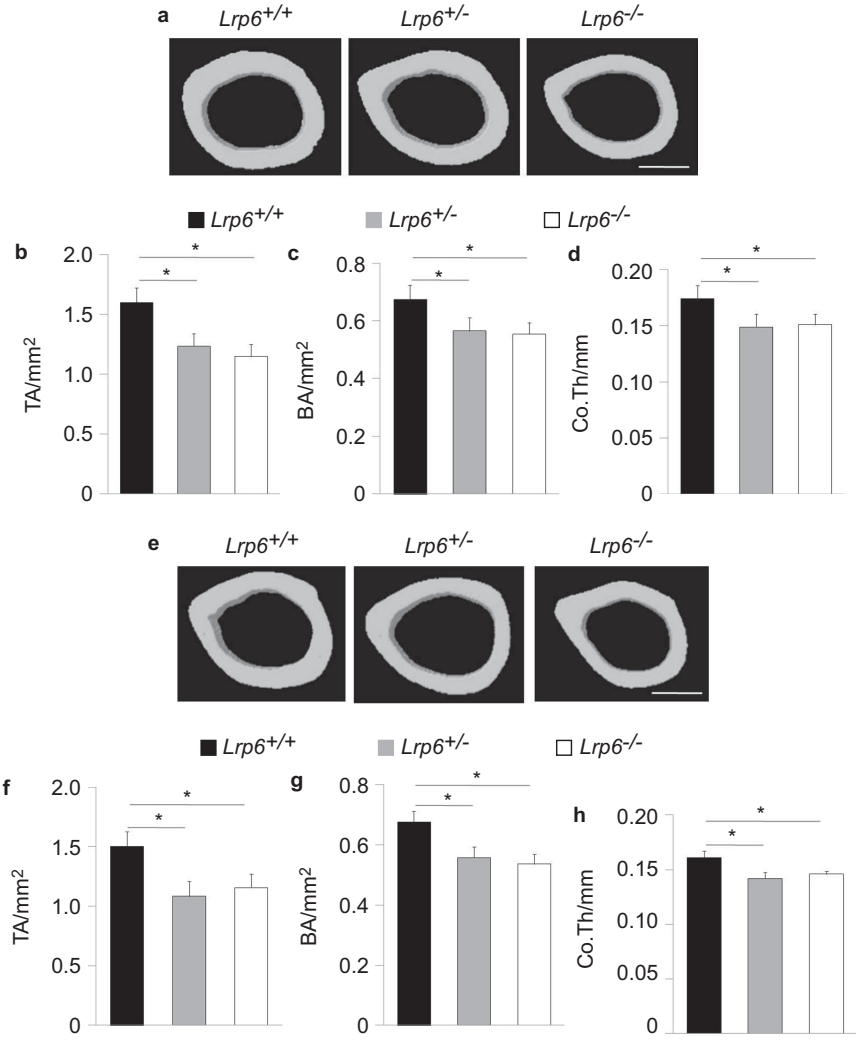

Figure 3. Mice with LRP6 deletion in nestin$^+$ MSCs exhibit low bone mass in cortical bone. (**a**) Representative μCT images of cross-sections of femoral mid-diaphyses from 3 month-old male *Lrp6*$^{+/+}$, *Lrp6*$^{+/-}$ and *Lrp6*$^{-/-}$ mice. Scale bar=500 μm. (**b–d**) quantitative analysis of cross-sections of femoral mid-diaphyses from 3-month-old male *Lrp6*$^{+/+}$, *Lrp6*$^{+/-}$ and *Lrp6*$^{-/-}$ mice. Total area with the periosteal circumference (TA) (**b**), cortical bone area (BA) (**c**) and cortical bone thickness (Co.Th) (**d**). (**e**) Representative μCT images and quantitative analysis of cross-sections of femoral mid-diaphyses from 3-month-old female mice. Scale bar=500 μm. (**f–h**) quantitative analysis of cross-sections of femoral mid-diaphyses from 3-month-old female *Lrp6*$^{+/+}$, *Lrp6*$^{+/-}$ and *Lrp6*$^{-/-}$ mice. Total area with the periosteal circumference (TA) (**f**), cortical bone area (BA) (**g**) and cortical bone thickness (Co.Th) (**h**). n=10, *P<0.01, **P<0.001, *vs. Lrp6*$^{+/+}$ group.

Bone marrow MSCs with LRP6 deletion had reduced rate of survival and diminished ability of proliferation and colony forming

We examined the alterations of bone marrow nestin$^+$ MSCs in LRP6 mutant mice. Consistent with previous reports,[23] nestin$^+$ MSCs exhibited perivascular localization in bone marrow detected by immunofluorescence staining (Figure 6a). By quantification of the perivascular nestin$^+$ MSCs, we found reduced number of the cells in bone marrow of *Lrp6*$^{+/-}$ and *Lrp6*$^{-/-}$ mice (Figure 6b). The same numbers MSCs isolated from bone marrow were then seeded for a CFU-F assay. A decrease in the number of the formed colonies of MSCs from mutant mice was observed relative to WT mice were observed (Figure 6c). The cells from *Lrp6*$^{+/-}$ and *Lrp6*$^{-/-}$ mice lost their small spindle shape and turned into elongated bigger size when the same numbers of cells were seeded for each group and cultured for several days. Especially, the cells from *Lrp6*$^{-/-}$ mice showed much elongated and parallel-oriented clusters (Figure 6d). The results indicated that the cells may have declined growth/proliferation capacity and/or decreased survival rate after LRP6 is deleted from the cells. Indeed, cell growth and proliferation detected by population doubling time (Figure 6e) and BrdU incorporation were significantly decreased (Figure 6f and 6g). The percentage of the dead cells detected by typan blue staining was also increased in cells with LRP6 deletion (Figure 6h). Collectively, the results

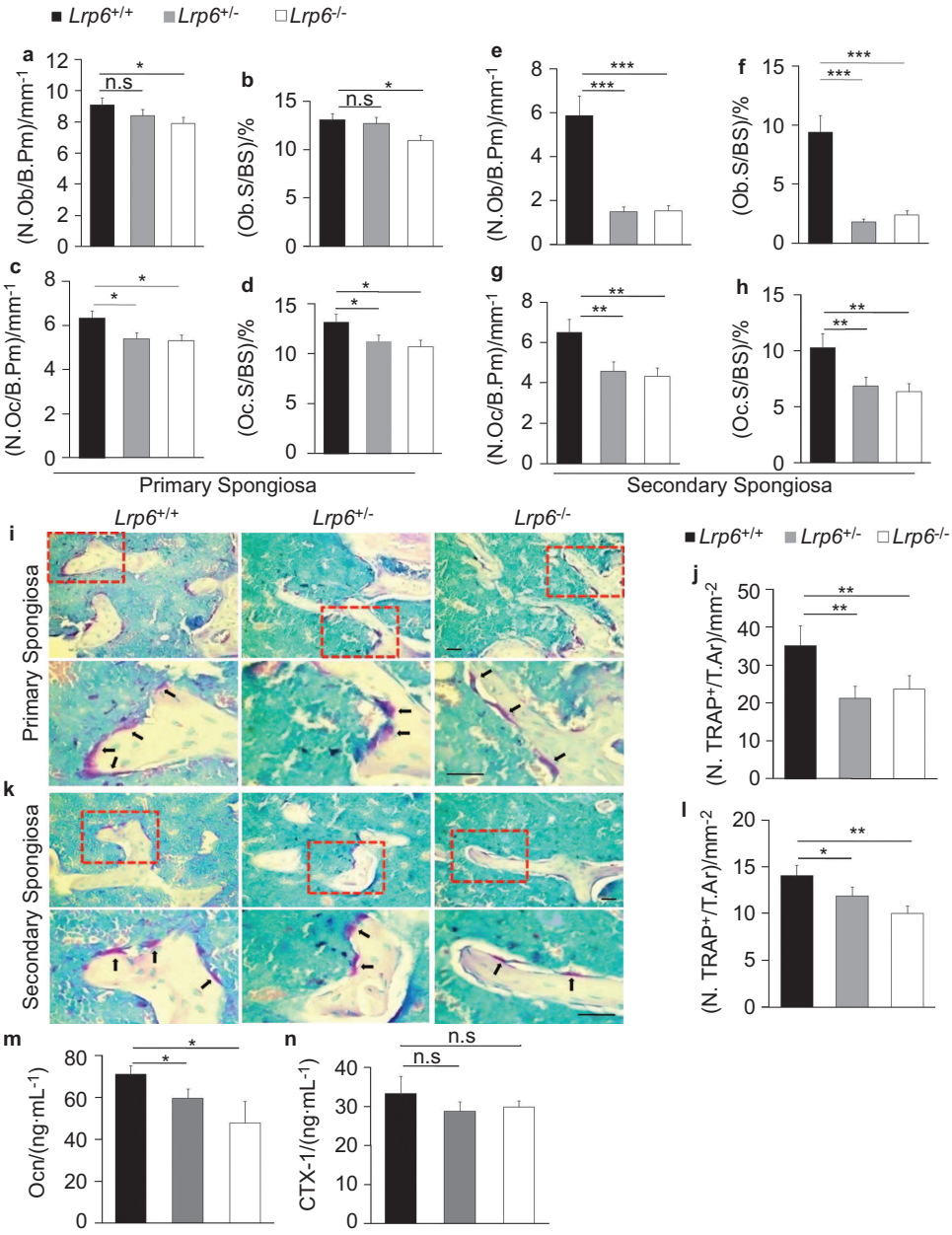

Figure 4. LRP6 deletion in nestin^{+} MSCs results in dramatic decreased osteoblast numbers. (**a–h**) Bone histomorphometric analysis of the primary spongiosa area (**a–d**) and secondary spongiosa area (**e–h**) of femur from 3-month-old male *Lrp6*$^{+/+}$, *Lrp6*$^{+/-}$ and *Lrp6*$^{-/-}$ mice. Number of osteoblasts per bone perimeter (N.Ob/B.Pm) (**a** and **e**), osteoblast surface per bone surface (Ob.S/BS) (**b** and **f**), number of osteoclasts per bone perimeter (N.Oc/B.Pm) (**c** and **g**) and osteoclast surface per bone surface (Oc.S/BS) (**d** and **h**). A total of three femur sections from each mouse, and six mice per treatment group were analyzed. *P<0.05, **P<0.01, ***P<0.001, *vs. Lrp6*$^{+/+}$ group. (**i–l**) Representative TRAP staining and quantitative analysis of the primary spongiosa area (**i** and **j**) and secondary spongiosa area (**k** and **l**) of trabecular bone sections from distal femur. Arrows, TRAP^{+} cells. Scale bars=100 μm. Number of TRAP-positive cells per mm^{2} tissue area (N.TRAP^{+} cells/T.Ar). A total of three femur sections from each mouse, and six mice per treatment group were analyzed. *P<0.05, **P<0.01, ***P<0.001, *vs. Lrp6*$^{+/+}$ group. (**m** and **n**) Serum levels of Ocn (**m**) and CTX-I (**n**) in wild-type *Lrp6*$^{+/+}$, *Lrp6*$^{+/-}$ and *Lrp6*$^{-/-}$ mice. n=4; *P<0.05. Data are presented as mean±s.e.m. CTX-I, c-terminal telopeptide of type-1 collagen; Ocn, osteocalcin.

suggest that the primary role of LRP6 in MSCs is to maintain the survival and proliferative capacity of the cells.

DISCUSSION

By employing genetic deletion of *Lrp6* in nestin^{+} MSCs, we have established that this transmembrane protein is crucial for bone marrow MSCs to preserve their growth and proliferation potential, and therefore, is required for the sufficient replenishment of osteoblasts and the maintenance of bone mass. The results provide new evidence for the role of LRP6 as a positive regulator of osteoblastic bone formation during postnatal skeletal growth and

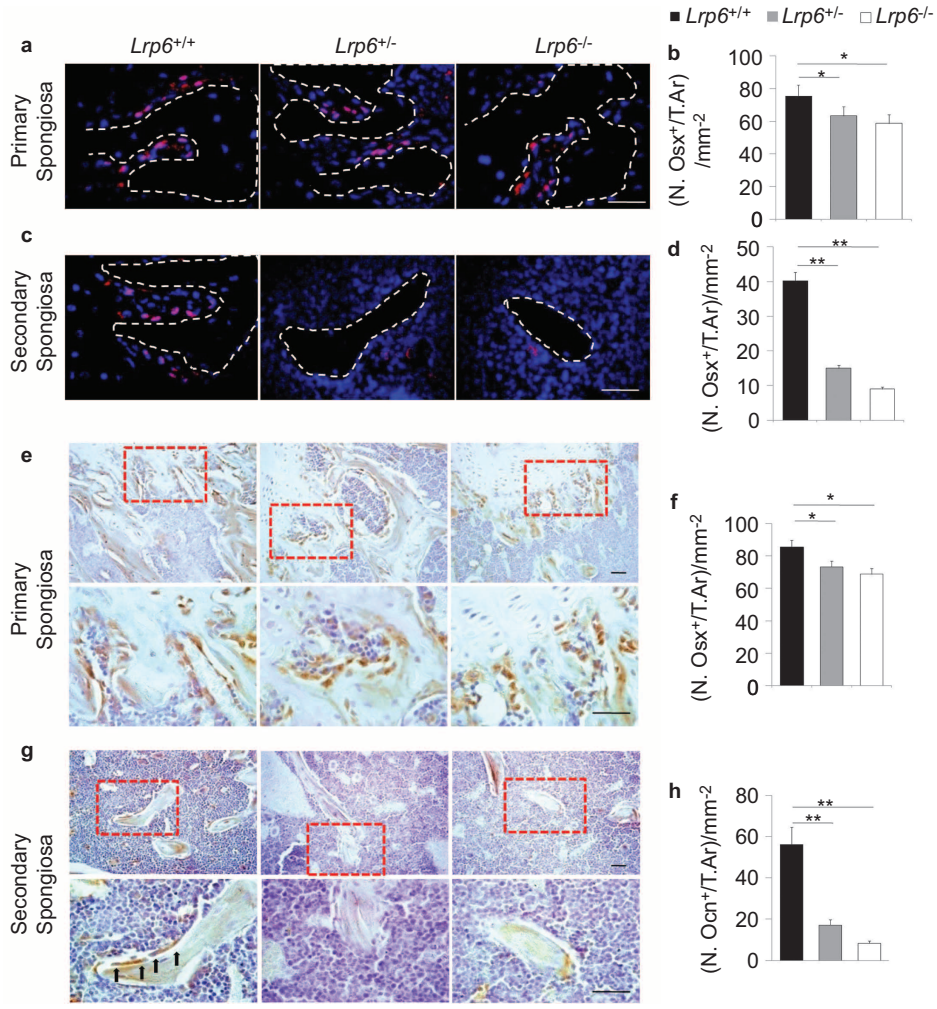

Figure 5. Mice with LRP6 deletion in nestin$^+$ MSCs have decreased osteoblastogenesis in bone. (**a** and **b**) Representative immunofluorescence staining and quantitative analysis of Osx in the primary spongiosa area (**a** and **b**) and secondary spongiosa area (**c** and **d**) of in femur sections of 3-month-old male *Lrp6*$^{+/+}$, *Lrp6*$^{+/-}$ and *Lrp6*$^{-/-}$ mice. Positive cells are in red. Nuclei are in blue. Scale bars=100 μm. Number of Osx-positive cells per mm^2 tissue area (N.Osx$^+$ cells/T.Ar). (**e**–**h**) Representative immunohistochemical staining and quantitative analysis of Ocn in the primary spongiosa area (**e** and **f**) and secondary spongiosa area (**g** and **h**) of in femur sections of 3-month-old male *Lrp6*$^{+/+}$, *Lrp6*$^{+/-}$ and *Lrp6*$^{-/-}$ mice. Scale bars=100 μm. Number of Ocn-positive cells per mm^2 tissue area (N.Ocn$^+$ cells/T.Ar). A total of three femur sections from each mouse, and five mice per treatment group were analyzed. **P*<0.05, ***P*<0.001, *vs. Lrp6*$^{+/+}$ group. Ocn, osteocalcin; Osx, osterix.

bone remodeling in adults. More importantly, the finding reveals that LRP6 regulates the function of osteoblastic lineage, at least partially, at stem cell level. The activities of LRP6 are modulated by a large number of hormones/growth factors that have bone anabolic effect such as PTH,[12,29–32] Wnts,[1–5] bone morphogenetic proteins (BMPs),[32] platelet-derived growth factor (PDGF)[33] as well as many extracellular proteins that negatively regulates osteoblastic bone formation including members of the Dickkopf family[34–36] and sclerostin.[37–40] Our finding suggests that regulation of the activities of bone marrow MSCs may be one of the major mechanisms by which these factors act on bone.

The normal survival of mice with MSC-specific *Lrp6* deletion, contrasting with the perinatal lethality of global *Lrp6* null/null mice,[2,10] suggests that LRP6 in nestin$^+$ MSCs is dispensible for embryonic development. However, mice with homozygous and heterozygous LRP6 deficiency in nestin$^+$ MSCs showed smaller size at 1 month of age, indicating that LRP6 in nestin$^+$ MSCs may play a role in skeletal development. A previous report showing that deletion of LRP6 alone specifically in the early mesenchyme, which contain precursors for the skeletal tissues, has little effect on embryonic skeletal development.[21] The discrepancy in phenotype between the two types of mutants was likely due to the different distribution of LRP6-deleted tissue using nestin-Cre and Dermo1-Cre-mediated recombination. Systemic characterization of the skeletal changes at different stages of embryonic development is necessary to delineate

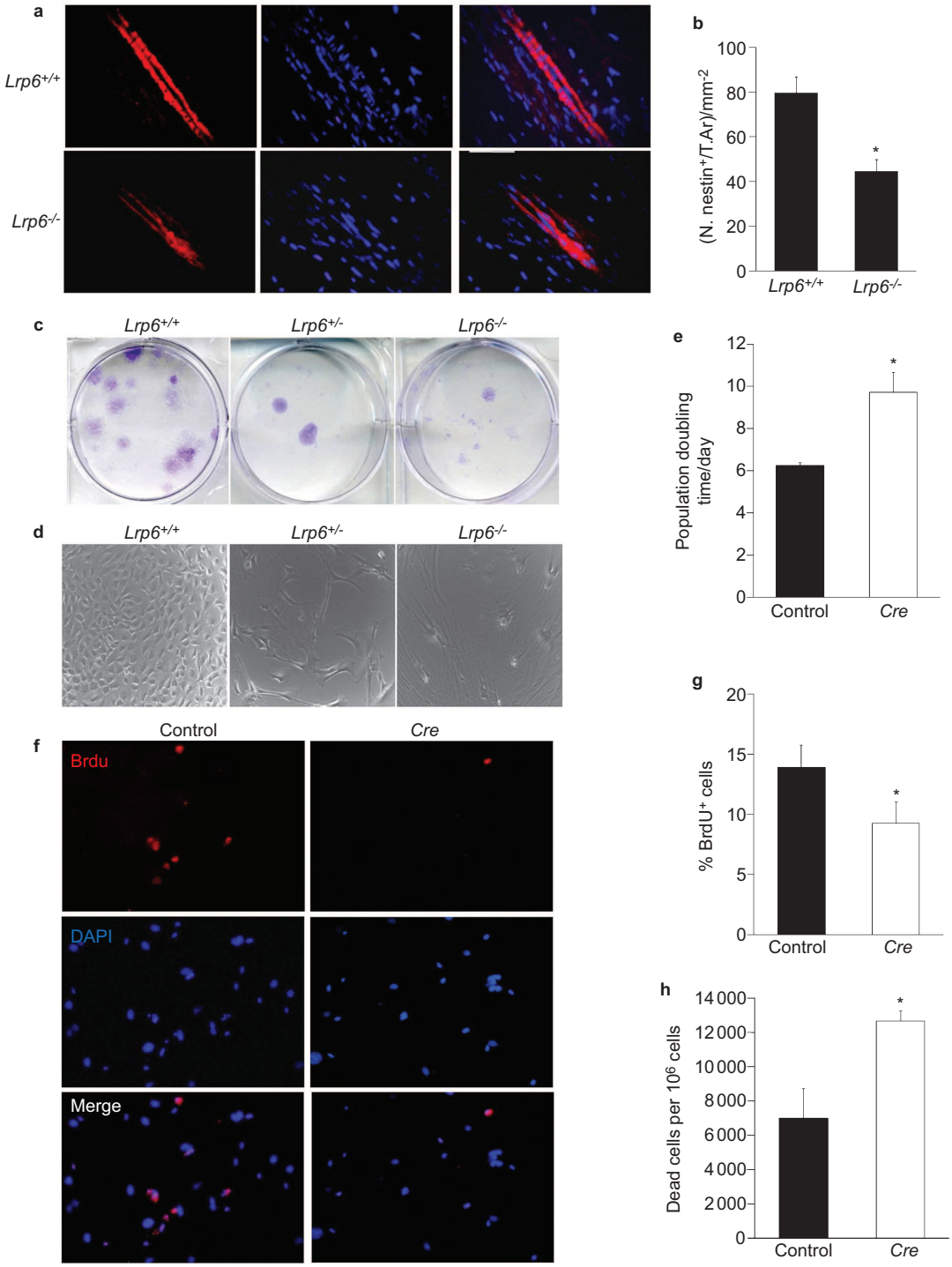

Figure 6. Bone marrow MSCs with LRP6 deletion had reduced rate of survival and diminished ability of proliferation and colony forming. (**a** and **b**) Representative immunofluorescence staining of nestin (red) in femur sections from male $Lrp6^{+/+}$ and $Lrp6^{-/-}$ mice (**a**). Scale bars=100 μm. Quantitative analysis of the percentage of nestin$^+$ cells per mm^2 tissue area (**b**). A total of three femur sections from each mouse, and five mice per treatment group were analyzed. *P<0.001, *vs.* $Lrp6^{+/+}$ group. (**c**) Colony-forming potential of bone marrow cells from 3-month-old male $Lrp6^{+/+}$, $Lrp6^{+/-}$ and $Lrp6^{-/-}$ mice. (**d**) Representative phase-contrast micrographs of bone marrow MSCs sorted from 3-month-old male $Lrp6^{+/+}$, $Lrp6^{+/-}$ and $Lrp6^{-/-}$ mice. (**e**) Population doubling time in days of MSCs infected with adenovirus containing GFP (control) or Cre between passage 1 (P1) and passage 2 (P2). n=5 for each treatment group; *P<0.001. (**f**) Representative immunofluorescence staining of BrdU (red) in MSCs infected with adenovirus containing GFP or Cre and labeled with BrdU. Nuclei were counterstained with DAPI (blue). (**g**) Quantitative analysis of the percentage of BrdU$^+$ cells out of the total cells. Cells were counted from four random high power fields per slides. n=5 slides for each treatment group; *P<0.001. (**h**) Quantitative analysis of the percentage of dead cells out of the total MSCs infected with adenovirus containing GFP (control) or Cre. n=5 for each treatment group; *P<0.001. BrdU, 5-bromo-2′-deoxyuridine; DAPI, 4′,6-diamidino-2-phenylindole; GFP, green fluorescent protein.

whether LRP6 in nestin$^+$ MSCs is required for embryonic skeletal development.

The phenotype of mice with MSC-specific LRP6 deletion is different from that of osteocalcin promoter-driven osteoblast-specific LRP6 knockout mice, which show unchanged body weight and femur length.[12] The two different phenotypes indicate that LRP6 in MSCs is important in the preservation of bone acquisition during postnatal skeletal growth and modeling, whereas LRP6 in mature osteoblasts primarily promotes bone formation during bone remodeling without affecting bone growth. Our data from the 3-month-old mutant mice also indicates that LRP6 in MSCs regulates osteoblastogenesis and bone formation during bone remodeling. Low bone mass and reduced osteoblast numbers in bone tissue were observed in 3-month-old mutant mice. Importantly, the reductions in osteoprogenitors and osteoblasts in bone tissue of mutant mice were much more dramatic at the active bone remodeling area, i.e., secondary spongiosa area *vs.* primary spongiosa area. Thus, MSC-specific LRP6 plays an important role in bone formation not only during bone growth in young mice, but also in bone remodeling in adults.

Bone formation in both skeletal growth/modeling and remodeling relies on the number and function of bone-forming osteoblasts. In fact, bone surface osteoblasts are non-replicative cells and require replenishment from bone marrow-derived MSCs,[20] suggesting that osteoblastic new bone formation depends on the activity of MSCs. Our *in vitro* finding that isolated MSCs from LRP6-deficient mice had decreased CFU-Fs and cell proliferation and prolonged population doubling time suggests that LRP6 is essential to preserve the growth/proliferation capacity of bone marrow MSCs, eventually leading to decreased osteoblast number and consequent bone formation. We realize that the nestin promoter-driven Cre may also delete LRP6 in neural stem cells/progenitor cells as nestin was originally described as a neuronal stem cell marker expressed during central nervous system development.[41–43] LRP6 null mice display a delay in the onset of dopamin precursor differentiation a defect in midbrain morphogenesis[44] and human LRP6 mutation is associated with late-onset Alzheimer's disease.[45] However, whether nestin$^+$ cell-specific LRP6 deletion causes severe brain abnormalities and whether the changes of brain indirectly impact on skeleton are to be characterized. In the present study, the significantly altered functions of bone marrow MSCs from the mutant mice in the *in vitro* culture experiments strongly suggest that the functional decline of bone marrow MSCs after LRP6 deletion contributes directly to the skeletal defects in the mutant mice. Future characterization of the bone phenotype of mice with MSC-specific LRP6 deletion in an inducible nestin-Cre system may help to limit the potential involvement of the neural stem cells/progenitor cells and further define the role of MSC-specific LRP6 in bone.

Our results also show decreased osteoclast numbers and activity in bone tissue of 3-month-old mutant mice. It is most likely that the decreased osteoclastogenesis in these mutant mice is a secondary effect that is caused by the osteoblastic bone formation changes. The fact that significantly reduced serum osteoblast marker osteocalcin and unchanged serum osteoclast marker CTX-1 further supports this concept. To maintain bone mass and bone quality, osteoclast bone resorption is tightly coupled with osteoblastic bone formation during bone remodeling, which requires a fine regulation by humoral factors or molecules mediating the communication among these two types of bone cells. Therefore, the dramatically reduced osteoblast numbers and activity may change the production of the communication factor(s) to suppress osteoclast activity. Specifically, LRP6 deficiency may cause inactivation of β-catenin signaling in osteoblastic lineage of cells, leading to reduced Receptor activator of nuclear factor kappa-B ligand (RANKL) production and inhibited osteoclastogenesis. Additional studies would be required to test this idea more definitively.

In conclusion, our studies demonstrate that LRP6 in bone marrow MSCs is required for their survival and proliferative potential as well as the consequent osteoblastic bone formation during both postnatal bone growth/modeling and bone remodeling in adults.

AUTHORS' CONTRIBUTIONS

Changjun Li performed the experiments. Bart O Williams and Xu Cao analyzed the results and proofread the manuscript. Mei Wan supervised and designed the experiments, analyzed results and wrote the article.

Conflict of Interest

The authors declare no conflict of interest.

Acknowledgements

This work was supported by National Institutes of Health Grant DK083350 to M. W.

References

1 Tamai K, Semenov M, Kato Y *et al.* LDL-receptor-related proteins in Wnt signal transduction. *Nature* 2000; **407**: 530–535.
2 Pinson KI, Brennan J, Monkley S, Avery BJ, Skarnes WC. An LDL-receptor-related protein mediates Wnt signalling in mice. *Nature* 2000; **407**: 535–538.
3 Huelsken J, Birchmeier W. New aspects of Wnt signaling pathways in higher vertebrates. *Curr Opin Genet Dev* 2001; **11**: 547–553.
4 Mao J, Wang J, Liu B *et al.* Low-density lipoprotein receptor-related protein-5 binds to Axin and regulates the canonical Wnt signaling pathway. *Mol Cell* 2001; **7**: 801–809.
5 Tamai K, Zeng X, Liu C *et al.* A mechanism for Wnt coreceptor activation. *Mol Cell* 2004; **13**: 149–156.

6 Mani A, Radhakrishnan J, Wang H *et al.* LRP6 mutation in a family with early coronary disease and metabolic risk factors. *Science* 2007; **315**: 1278–1282.
7 Singh R, Smith E, Fathzadeh M *et al.* Rare nonconservative LRP6 mutations are associated with metabolic syndrome. *Hum Mutat* 2013; **34**: 1221–1225.
8 van Meurs JB, Rivadeneira F, Jhamai M *et al.* Common genetic variation of the low-density lipoprotein receptor-related protein 5 and 6 genes determines fracture risk in elderly white men. *J Bone Miner Res* 2006; **21**: 141–150.
9 van Meurs JB, Trikalinos TA, Ralston SH *et al.* Large-scale analysis of association between LRP5 and LRP6 variants and osteoporosis. *JAMA* 2008; **299**: 1277–1290.
10 Kelly OG, Pinson KI, Skarnes WC. The Wnt co-receptors Lrp5 and Lrp6 are essential for gastrulation in mice. *Development* 2004; **131**: 2803–2815.
11 Holmen SL, Giambernardi TA, Zylstra CR *et al.* Decreased BMD and limb deformities in mice carrying mutations in both Lrp5 and Lrp6. *J Bone Miner Res* 2004; **19**: 2033–2040.
12 Li C, Xing Q, Yu B *et al.* Disruption of LRP6 in osteoblasts blunts the bone anabolic activity of PTH. *J Bone Miner Res* 2013; **28**: 2094–2108.
13 Riddle RC, Diegel CR, Leslie JM *et al.* Lrp5 and Lrp6 exert overlapping functions in osteoblasts during postnatal bone acquisition. *PLoS ONE* 2013; **8**: e63323.
14 Gong Y, Slee RB, Fukai N *et al.* LDL receptor-related protein 5 (LRP5) affects bone accrual and eye development. *Cell* 2001; **107**: 513–523.
15 Little RD, Recker RR, Johnson ML. High bone density due to a mutation in LDL-receptor-related protein 5. *N Engl J Med* 2002; **347**: 943–944.
16 Little RD, Carulli JP, del Mastro RG *et al.* A mutation in the LDL receptor-related protein 5 gene results in the autosomal dominant high-bone-mass trait. *Am J Hum Genet* 2002; **70**: 11–19.
17 Boyden LM, Mao J, Belsky J *et al.* High bone density due to a mutation in LDL-receptor-related protein 5. *N Engl J Med* 2002; **346**: 1513–1521.
18 Kokubu C, Heinzmann U, Kokubu T *et al.* Skeletal defects in ringelschwanz mutant mice reveal that Lrp6 is required for proper somitogenesis and osteogenesis. *Development* 2004; **131**: 5469–5480.
19 Kubota T, Michigami T, Sakaguchi N *et al.* Lrp6 hypomorphic mutation affects bone mass through bone resorption in mice and impairs interaction with Mesd. *J Bone Miner Res* 2008; **23**: 1661–1671.
20 Park D, Spencer JA, Koh BI *et al.* Endogenous bone marrow MSCs are dynamic, fate-restricted participants in bone maintenance and regeneration. *Cell Stem Cell* 2012; **10**: 259–272.
21 Joeng KS, Schumacher CA, Zylstra-Diegel CR, Long F, Williams BO. Lrp5 and Lrp6 redundantly control skeletal development in the mouse embryo. *Dev Biol* 2011; **359**: 222–229.
22 Lendahl U, Zimmerman LB, McKay RD. CNS stem cells express a new class of intermediate filament protein. *Cell* 1990; **60**: 585–595.
23 Mendez-Ferrer S, Michurina TV, Ferraro F *et al.* Mesenchymal and haematopoietic stem cells form a unique bone marrow niche. *Nature* 2010; **466**: 829–834.
24 Zylstra CR, Wan C, VanKoevering KK *et al.* Gene targeting approaches in mice: assessing the roles of LRP5 and LRP6 in osteoblasts. *J Musculoskelet Neuron Interact* 2008; **8**: 291–293.
25 Wu X, Pang L, Lei W *et al.* Inhibition of Sca-1-positive skeletal stem cell recruitment by alendronate blunts the anabolic effects of parathyroid hormone on bone remodeling. *Cell Stem Cell* 2010; **7**: 571–580.
26 Zhang M, Xuan S, Bouxsein ML *et al.* Osteoblast-specific knockout of the insulin-like growth factor (IGF) receptor gene reveals an essential role of IGF signaling in bone matrix mineralization. *J Biol Chem* 2002; **277**: 44005–44012.
27 Canalis E, Parker K, Feng JQ, Zanotti S. Osteoblast lineage-specific effects of notch activation in the skeleton. *Endocrinology* 2013; **154**: 623–634.
28 Courtland HW, Elis S, Wu Y *et al.* Serum IGF-1 affects skeletal acquisition in a temporal and compartment-specific manner. *PLoS ONE* 2011; **6**: e14762.
29 Wan M, Yang C, Li J *et al.* Parathyroid hormone signaling through low-density lipoprotein-related protein 6. *Genes Dev* 2008; **22**: 2968–2979.
30 Wan M, Li J, Herbst K *et al.* LRP6 mediates cAMP generation by G protein-coupled receptors through regulating the membrane targeting of Galpha(s). *Sci Signal* 2011; **4**: ra15.
31 Shi C, Li J, Wang W, Cao W, Cao X, Wan M. Antagonists of LRP6 regulate PTH-induced cAMP generation. *Ann NY Acad Sci* 2011; **1237**: 39–46.
32 Yu B, Zhao X, Yang C *et al.* Parathyroid hormone induces differentiation of mesenchymal stromal/stem cells by enhancing bone morphogenetic protein signaling. *J Bone Miner Res* 2012; **27**: 2001–2014.
33 Ren S, Johnson BG, Kida Y *et al.* LRP-6 is a coreceptor for multiple fibrogenic signaling pathways in pericytes and myofibroblasts that are inhibited by DKK-1. *Proc Natl Acad Sci USA* 2013; **110**: 1440–1445.
34 Semenov MV, Tamai K, Brott BK, Kuhl M, Sokol S, He X. Head inducer Dickkopf-1 is a ligand for Wnt coreceptor LRP6. *Curr Biol* 2001; **11**: 951–961.
35 Mao B, Wu W, Li Y *et al.* LDL-receptor-related protein 6 is a receptor for Dickkopf proteins. *Nature* 2001; **411**: 321–325.
36 Bafico A, Liu G, Yaniv A, Gazit A, Aaronson SA. Novel mechanism of Wnt signalling inhibition mediated by Dickkopf-1 interaction with LRP6/Arrow. *Nat Cell Biol* 2001; **3**: 683–686.
37 Semenov M, Tamai K, He X. SOST is a ligand for LRP5/LRP6 and a Wnt signaling inhibitor. *J Biol Chem* 2005; **280**: 26770–26775.
38 Semenov MV, He X. LRP5 mutations linked to high bone mass diseases cause reduced LRP5 binding and inhibition by SOST. *J Biol Chem* 2006; **281**: 38276–38284.
39 Li X, Zhang Y, Kang H *et al.* Sclerostin binds to LRP5/6 and antagonizes canonical Wnt signaling. *J Biol Chem* 2005; **280**: 19883–19887.
40 Ellies DL, Viviano B, McCarthy J *et al.* Bone density ligand, Sclerostin, directly interacts with LRP5 but not LRP5G171V to modulate Wnt activity. *J Bone Miner Res* 2006; **21**: 1738–1749.
41 Bonaguidi MA, Wheeler MA, Shapiro JS *et al. In vivo* clonal analysis reveals self-renewing and multipotent adult neural stem cell characteristics. *Cell* 2011; **145**: 1142–1155.
42 Burns KA, Ayoub AE, Breunig JJ *et al.* Nestin-CreER mice reveal DNA synthesis by nonapoptotic neurons following cerebral ischemia hypoxia. *Cereb Cortex* 2007; **17**: 2585–2592.
43 Burns KA, Murphy B, Danzer SC, Kuan CY. Developmental and post-injury cortical gliogenesis: a genetic fate-mapping study with Nestin-CreER mice. *Glia* 2009; **57**: 1115–1129.
44 Castelo-Branco G, Andersson ER, Minina E *et al.* Delayed dopaminergic neuron differentiation in Lrp6 mutant mice. *Dev Dyn* 2010; **239**: 211–221.
45 de Ferrari GV, Papassotiropoulos A, Biechele T *et al.* Common genetic variation within the low-density lipoprotein receptor-related protein 6 and late-onset Alzheimer's disease. *Proc Natl Acad Sci USA* 2007; **104**: 9434–9439.